(Received 29 November 2025, Accepted 21 January 2026, Scheduled 8 May 2026)

Design of a DGS-Loaded Scannable Cosecant^2-Shaped Pattern Generating Phased Array Antenna with Improved Cross Polarization

Rajeev Jyoti, Amalendu Patnaik, Gaurav Kumar*, Pratik Mevada, and Gaurav Ahuja

Space Applications Centre, India

ABSTRACT: This manuscript describes the design of a scannable Cosecant^2-Shaped Pattern Generating Phased Array Antenna (PAA) intended for airborne synthetic aperture radar (SAR). The Cosecant^2 Shape avoids the requirement of sensitivity time control correction at the receiver side. A C-band linear array antenna consisting of 16 elements is designed, analyzed, developed, and characterized. The array antenna is embedded with a U-slot and Defected Ground Structure (DGS) integrated microstrip elements. The introduction of a DGS provides a 6.5 dB improvement in cross-polarization levels when scanning. Additionally, the null perturbation technique is employed to synthesize the excitation coefficients for the Cosecant^2-Shaped pattern, aiming to achieve the minimum current taper ratio. These synthesized coefficients are combined with a progressive phase for beams that can scan within a $\pm 30^\circ$ angular range. The proposed linear array, along with its excitation and phasing network, has also been developed and characterized in an anechoic chamber.

1. INTRODUCTION

The radar industry is growing rapidly and is driving the demand for low-profile, reconfigurable, and shaped-beam antennas. This requirement can be met with an antenna element that provides independent amplitude and phase control [1]. Balanis [1] provides an in-depth examination of various array configurations, including uniform, nonuniform linear, circular, and rectangular arrays. Bhattacharya [2] further investigated triangular and rectangular lattice configurations in phased-array antennas, highlighting their unique attributes and performance characteristics.

The existing literature on phased-array antennas offers critical insights into key aspects, including scanning mechanisms, scan loss, scan blindness, grating lobes, and mutual coupling. Mailloux extensively covers these array parameters, providing a comprehensive overview of practical implications [3]. Furthermore, the authors elucidated the relationship between the active element pattern and the radiation characteristics of phased arrays [4].

A linear phased array is a key component of modern radar systems, which employs electronic beam steering and dynamic pattern shaping. Among the various techniques, cosecant^2 pattern has been widely used as a shaped beam pattern for air surveillance radar systems. The main advantage of the cosecant^2 pattern is its ability to provide a consistent signal strength to the receiver as a target moves at a constant height within the beam, thus improving the system's detection capabilities across a wide range of elevations. The cosecant^2-shaped pattern can also be used in Synthetic Aperture Radar (SAR) systems, offering high-resolution imaging of the Earth's surface, which is essential for remote sensing, mapping, and environmental monitoring. The use of such a shaped pattern for SAR drastically reduces the receiver's complexity. Currently, several methods are available for achieving cosecant^2 beamforming [5–15]. Techniques such as the synthesis pattern method [5], differential evolution algorithm [6], and genetic algorithm [7] were employed to determine the required amplitude and phase settings for the elements, enabling the creation of the desired radiation pattern. A hybrid technique that combines differential evolution with continuous ant colony optimization to generate the cosecant^2 pattern through the phase-only synthesis of a symmetrical antenna array was described in [9].

Another important technology being developed to improve the performance of array antennas is the Defective Ground Structure (DGS), which is widely used to generate circular polarization, suppress cross-polarization, and improve bandwidth [14–21]. In [14], the authors addressed cosecant^2 beam shaping using a U-slot to maximize power transmission efficiency. However, the manuscript did not mention cross polarization, the effect of the DGS, or the scanning of such a shaped beam. The authors of [15] investigated the fundamentals, analysis, and applications of defective ground structures (DGSs). They highlighted the advantages of various DGS geometries and their practical applications in contemporary wireless systems. The authors used orthogonally placed rectangular slots to achieve circular polarization in the L-band [16]. Guha et al. used a circular-slot DGS to improve the cross-polarization of a microstrip antenna by 5–8 dB [17]. Moreover, Dwivedy briefly summarized the impact and probable applications of a DGS in microstrip antennas [18].

* Corresponding author: Gaurav Kumar (gaurav.kr2802@gmail.com).

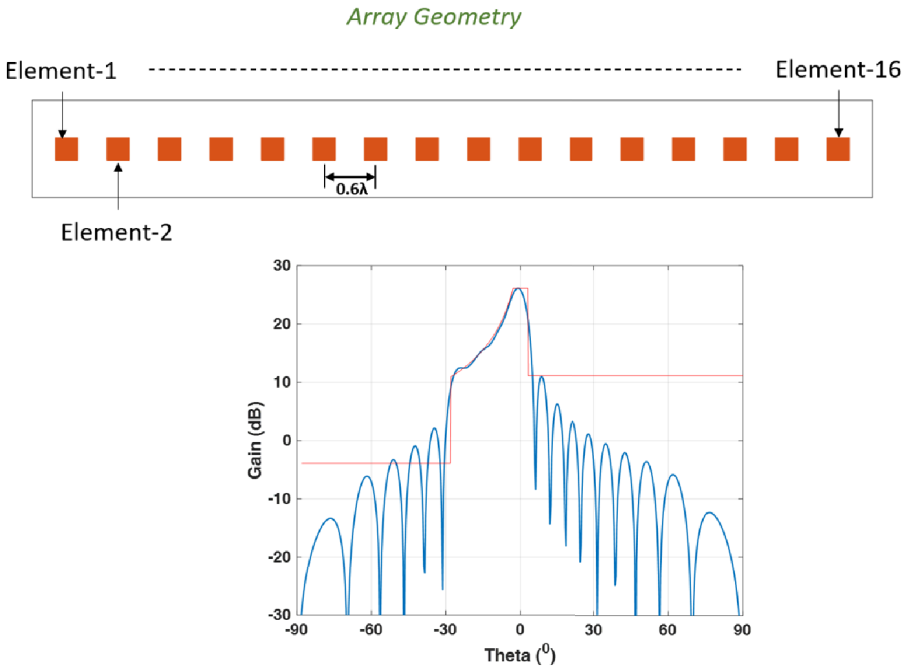

FIGURE 1. Array geometry and generated cosecant^2 pattern.

This work delves into the design of a linear U-slot and DGS-loaded patch array and into the generation and scanning of a cosecant^2 beam. Although extensive research has been conducted on the synthesis of cosecant^2 patterns, the literature lacks an investigation of scanned cosecant^2 beams. This is particularly important for airborne synthetic aperture radar (SAR), where scanning capabilities are necessary for aircraft banking operations. In addition, such scanning can help mitigate real-time aircraft jitter. This study addresses this technical gap by analyzing the performance of cosecant^2 beams during scanning implemented on a C-band 16-element linear array antenna. The authors also improved cross-polarization by introducing a DGS and U-slots. The manuscript contains five sections. Section 2 describes the synthesis of the cosecant^2 pattern. Section 3 briefly discusses the antenna design. Section 4 focuses on the design of the feed network, and the simulated and measured results are presented in Section 5, followed by the conclusion in Section 6.

2. SYNTHESIS OF COSECANT^2-SHAPED RADIATION PATTERN

A 16-element linear array with 0.6λ inter-element spacing was chosen to create a cosecant^2 pattern. A null-perturbation-based synthesis approach has been adopted for the excitation-weight computation of array elements [3] to generate a cosecant^2-shaped pattern. The MATLAB-based code was developed to compute excitation weights and optimize them to minimize the current taper ratio (CTR) for a practical, realizable feed network. The maximum CTR for synthesis was 130, and the minimum CTR was 28. The synthesized weights are listed in Table 1. The array pattern of the 16-element array was computed

TABLE 1. Synthesized excitation coefficient.

Ele No.	Amplitude (dB)	Phase (°)	Ele No.	Amplitude (dB)	Phase (°)
1	−11.34	0	9	−6.55	−85.36
2	−12.31	−53.4	10	−5.05	−78.1
3	−9.62	−53.15	11	−5.22	−73.51
4	−10.94	−53.57	12	−4.38	−79.86
5	−10.64	−73.48	13	−1.65	−74.32
6	−8.33	−75.36	14	0	−53.45
7	−8.21	−70.22	15	−0.58	−26.95
8	−8.61	−78.76	16	−3.94	−2.36

using the well-known array factor Equation (1) [3].

$$F(\theta) = \sum_{n=1}^{N} w_n \cdot e^{-jnkd(sin\theta - \sin\theta_0)} \tag{1}$$

where N = Number of array elements, w_n = Complex excitation of the nth element, d = inter-element spacing, θ_0 = Beam scan angle, and k = wave number.

The 16-element array generating the cosecant^2 pattern is shown in Fig. 1, along with a cosecant^2 pattern mask (in red). Scanning of the synthesized cosecant^2 pattern is achieved by adding a progressive phase shift to the elements, based on the phase introduced for shaping, as per Equation (2). Here, the steering angle θ_0 is the angle at which the peak of the shaped beam must be shifted. With an element spacing of 0.6λ, the grating lobe-free scan range was limited to 30°.

$$\varphi_{i,scanned\ shaped\ pattern} = \varphi_{i,shaped\ pattern} + \varphi_{i,progressive\ phase} \tag{2}$$

where 'i' is the element number.

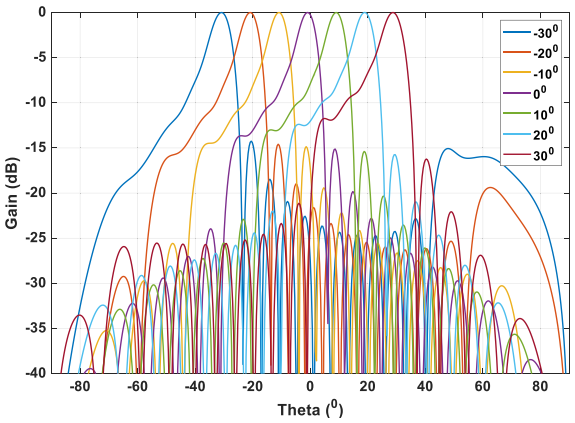

FIGURE 2. Scanned cosecant^2-shaped pattern.

Figure 2 shows plots of the phase-shifted cosecant^2-shaped pattern. The radiation patterns shown in Fig. 2 were computed by considering the excitation of each element via superposition of the shaped beam and progressive scanning.

3. U-SLOT BASED MICROSTRIP ANTENNA DESIGN

A coaxially fed rectangular microstrip patch operating at 6 GHz was designed and loaded with a U-shaped slot to improve antenna bandwidth. Fig. 3 shows the structure of a single element, designed on a 60 mil RO3003 ($\varepsilon_r = 2.94$ and $\tan\delta = 0.00012$).

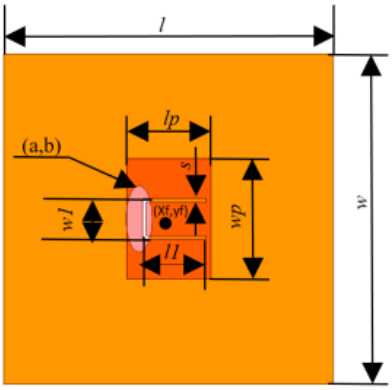

FIGURE 3. U-slot and DGS-loaded microstrip patch antenna.

The antenna dimensions are listed in Table 2. A linear array of 16 antenna elements was then designed with an inter-element spacing of 0.6λ, as shown in Fig. 4(a). Here, 0.6λ was chosen to facilitate beam scanning up to $\pm 30°$ without generating grating lobes. Furthermore, an ellipse-shaped DGS was introduced to improve the cross-polarization level. Fig. 4 shows the structure of a 16-element DGS-loaded U-slot patch array.

TABLE 2. Design parameters.

Parameter	Value	Parameter	Value
l	50 mm	l_1	9.5 mm
w	50 mm	w_1	6.1 mm
lp	12.7 mm	s	0.5 mm
wp	18.2 mm	xf	0 mm
a	10 mm	yf	0 mm
ε_r	2.94	b	4 mm
d	30 mm	hs	2.032 mm

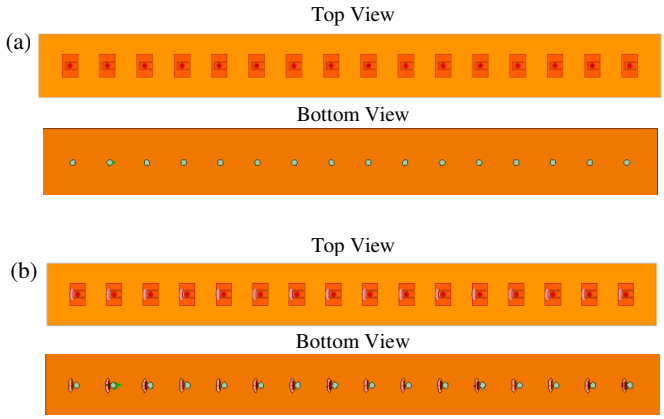

FIGURE 4. 16-element linear antenna array, (a) without a DGS and (b) with a DGS.

4. DESIGN OF FEED NETWORK FOR SHAPED BEAM

4.1. Excitation Network to Generate Cosecant^2-Shaped Pattern

Resistor (R)-loaded microstrip line-based feedlines were designed to excite the antenna elements with the required amplitude and phase. Fig. 5 shows the simulated model. The proposed excitation network was fabricated on a 1 mm thick FR4 substrate with ($\varepsilon_r = 4.3$ and a loss tangent of 0.02). Resistors were used to adjust the relative magnitudes of the excitation coefficients, and meandering was introduced to adjust the phases of the individual lines. The analyzed excitation amplitude and phase at 6 GHz for the 16 elements are listed in Table 3. From Table 3, a variation of 0.6 dB in amplitude and $\sim 50°$ in phase is observed as compared to the synthesized excitation coefficients. Such variations in amplitude and phase have a marginal impact on the shaped pattern.

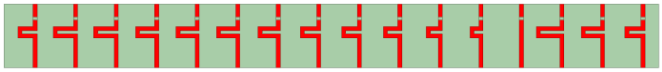

FIGURE 5. Feed network to generate cosecant^2 pattern.

4.2. Fixed Phase Reflection Type Phase Shifter Network

A quadrature hybrid reflection-type phase shifter is designed to provide a progressive phase shift for the beam scan. Fig. 6 shows the design of a microstrip line-based phase shifter built on a 1 mm thick FR4 substrate, where the output arms of the quadrature hybrid are shorted, and their lengths are varied to achieve an element-wise progressive phase shift. The phase shift was determined by the relative change in the length of the shorted microstrip line, as described by Equation (3).

$$\Delta\varphi = 2\pi\frac{\Delta L}{\lambda} \tag{3}$$

TABLE 3. Analyzed excitation coefficient.

Element No.	Amplitude	phase	Element No.	Amplitude	Phase
1	−11	0	9	−7.1	−78.9
2	−13	−60	10	−4.9	−81.4
3	−10.3	−58	11	−5.2	−70.4
4	−11.5	−56.4	12	−4.8	−81.4
5	−10.1	−75.4	13	−1.2	−72
6	−8	−78.2	14	−0.5	−53.0
7	−8.4	−74.6	15	−0.2	−26.4
8	−9.1	−84.1	16	−4.2	−5

TABLE 4. Variation in insertion loss with the length lrp.

Length lrp (mm)	Attenuation (dB)	Length lrp (mm)	Attenuation (dB)
1.5	−1.36	7.7	−2.30
2.1	−1.51	8.5	−2.12
3.3	−1.8	10.3	−1.77
4.1	−1.97	11.7	−1.57
5.5	−2.20	13.1	−1.57
6.3	−2.26	15	−1.92

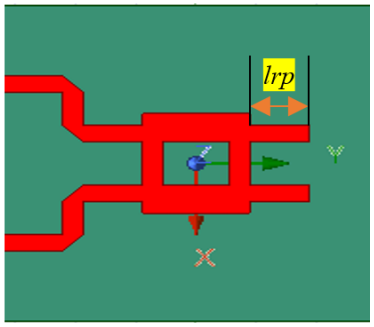

FIGURE 6. Quadrature hybrid phase shifter.

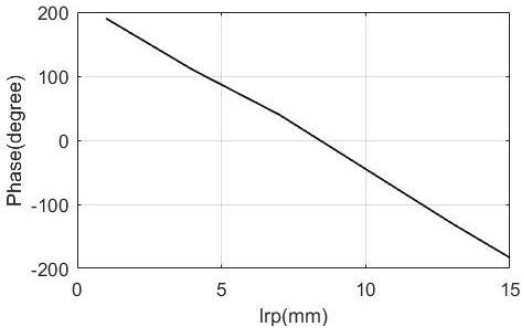

FIGURE 7. Variation of phase with lrp.

where ΔL is the relative change in length with respect to the adjusted smallest length, and λ is the operating wavelength. Here, the phase shifter was simulated for a relative change in length from 2 to 15 mm, and the corresponding phase variation is plotted in Fig. 7. The insertion loss also varies with the relative change in length and is tabulated in Table 4. From Table 4, it can be observed that the insertion loss is between −2.30 dB and −1.36 dB, which is an acceptable range. Moreover, a 16 nos. Quadrature hybrid-based phase shifters are populated on a single substrate and designed for −20°, −10°, 10°, and 20°. Fig. 8 shows the simulated structures.

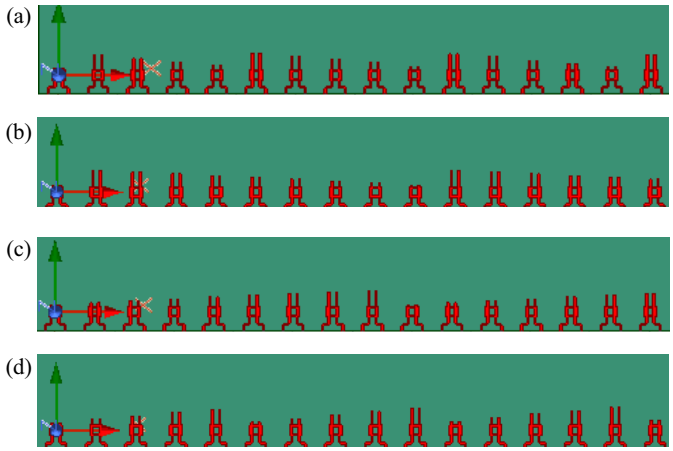

FIGURE 8. 16-element feed network for scanning at (a) −20°, (b) −10°, (c) +10° and (d) 20°.

5. RESULTS

5.1. Analysed Results

The simulated S_{11} parameters and radiation patterns of the U-slot-loaded antenna are shown in Fig. 9, comparing the scenarios with and without DGS loading. From Fig. 9, it can be observed that both configurations exhibit a 10 dB return loss bandwidth of 340 MHz. However, adding the DGS resulted in a 3.5 dB improvement in the cross-polarization level.

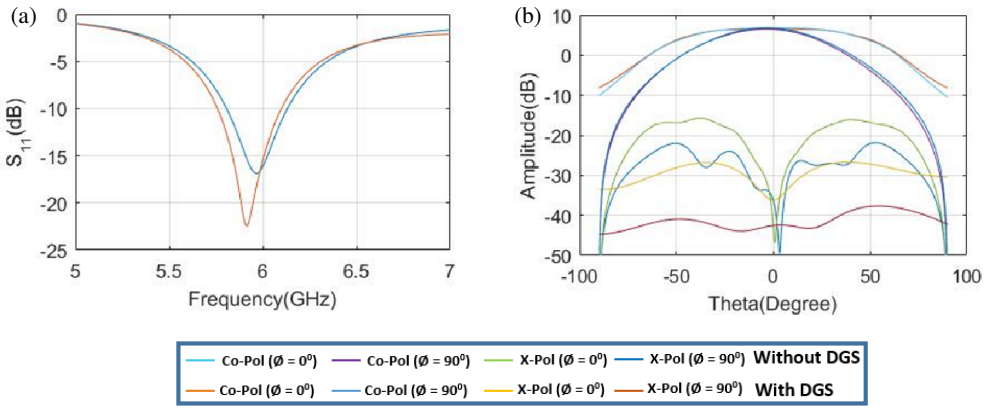

FIGURE 9. Simulated (a) S_{11} and (b) radiation pattern of a single antenna element without a DGS and with a DGS.

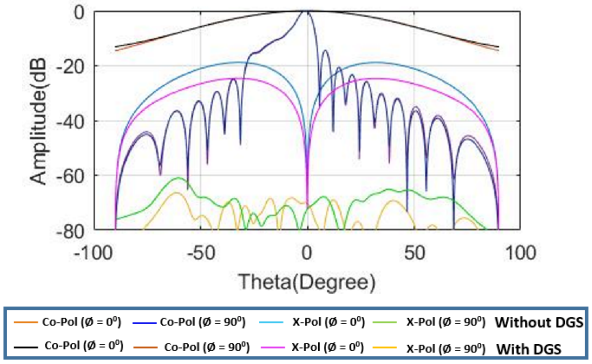

FIGURE 10. Radiation pattern of (a) uniformly excited and (b) cosecant^2-shaped beam of 16 element array with a DGS and without a DGS at 6 GHz.

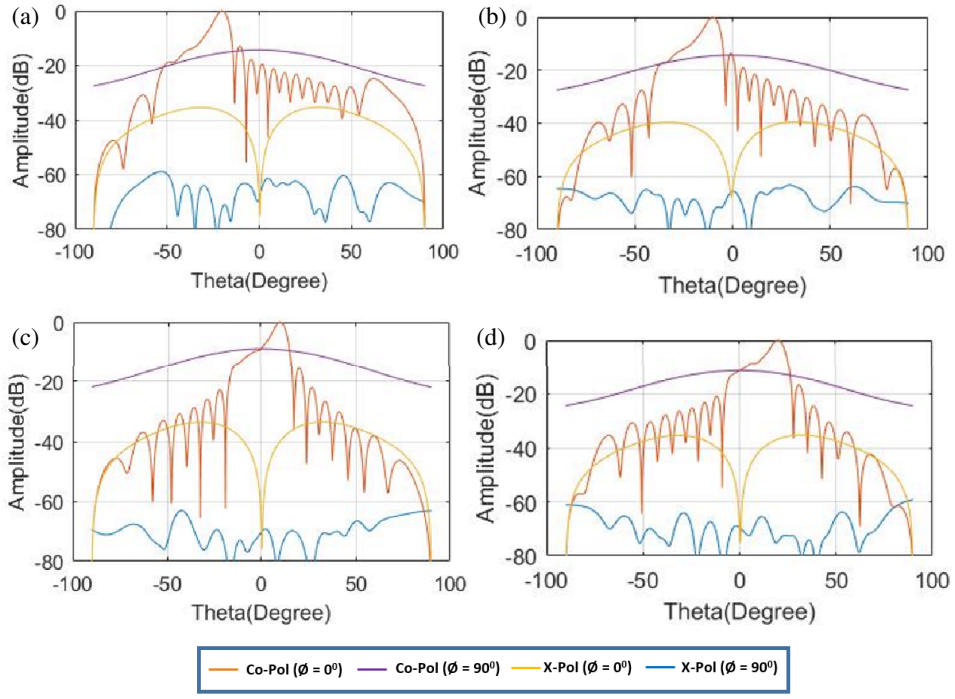

FIGURE 11. Cosecant^2 beam scanned at (a) $-20°$, (b) $-10°$, (c) $10°$ and (d) $20°$.

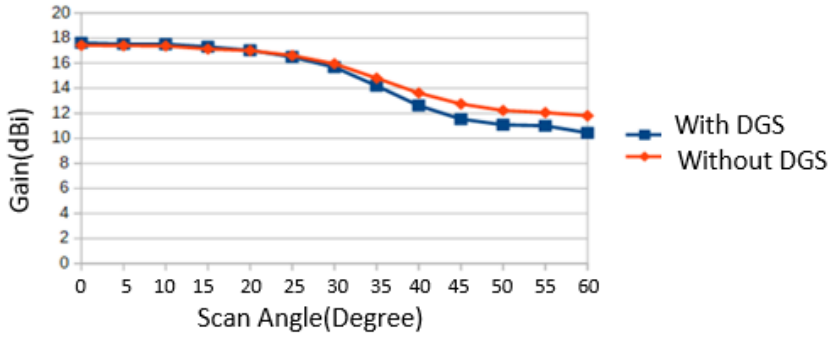

FIGURE 12. Gain variation with scan angle.

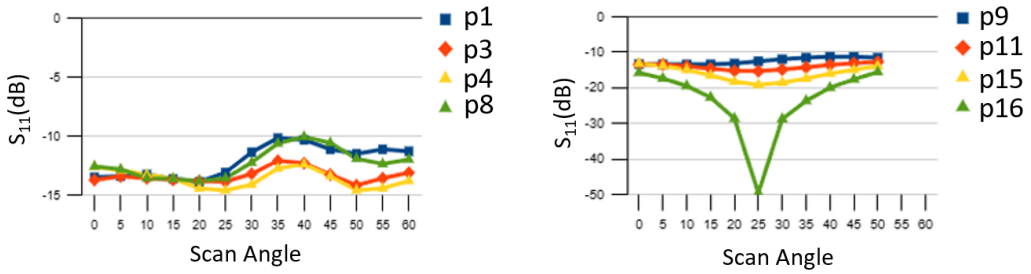

FIGURE 13. Active reflection coefficient of antenna elements.

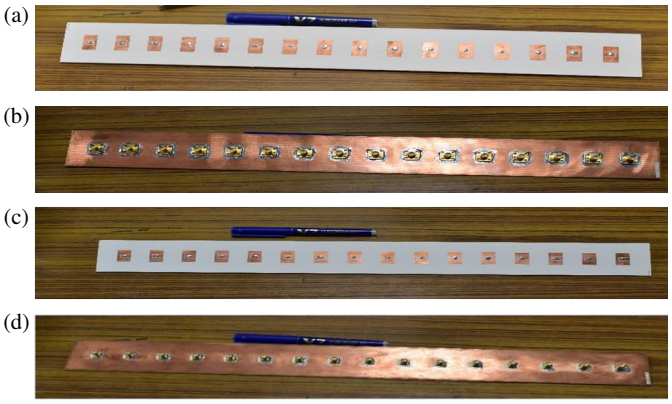

FIGURE 14. Fabricated 16-element array without a DGS, (a) top view, (b) bottom view, with a DGS, (c) top view, and (d) bottom view.

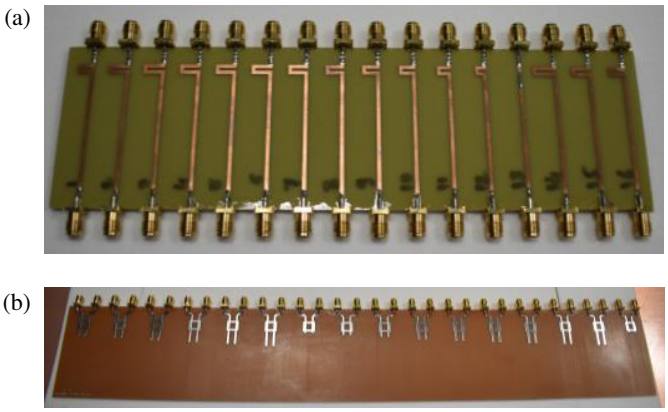

FIGURE 15. (a) Excitation network and (b) -20° phase shifter circuit.

A 16-element array of U-slot-loaded antennas, both with and without a DGS, was simulated using synthesized excitation to achieve a cosecant^2-shaped radiation pattern. Fig. 10 illustrates the simulated radiation patterns of the arrays under the no-scan condition. The peak gain for the array with the DGS was found to be 17.4 dBi. It is also noted that the inclusion of a DGS reduced array gain by 0.2 dB, a marginally significant effect. Additionally, as shown in Fig. 10, there is a clear 6.5 dB improvement in the cross-polarization.

Appropriate phase shifts are applied to the antenna elements to steer the beam to 10° and 20° (in both positive and negative directions), as illustrated in Fig. 11. The variation of antenna gain as a function of scan angle is presented in Fig. 12. It is observed that the gain variation remains negligible up to the scan angle of 30° for both configurations, i.e., with and without a DGS. Since the active reflection coefficient plays a critical role in the beam steering, the active S_{11} of all the antenna elements is evaluated and presented in Fig. 13. The results indicated that the active S_{11} is better than 10 dB for all 16 elements, confirming that the proposed linear array is free from scan blindness and suitable for beam-scanning applications.

5.2. Fabrication and Measured Results

A 16-element linear array antenna, with and without a defective ground structure (DGS), was fabricated and characterized across various beam-scanning scenarios. Fig. 14 illustrates the fabricated antenna structures, whereas Fig. 15 displays the excitation and phase-shifter networks designed to facilitate beam scanning of the shaped radiation pattern. Fig. 17 shows the measured return losses of several array elements. The figure

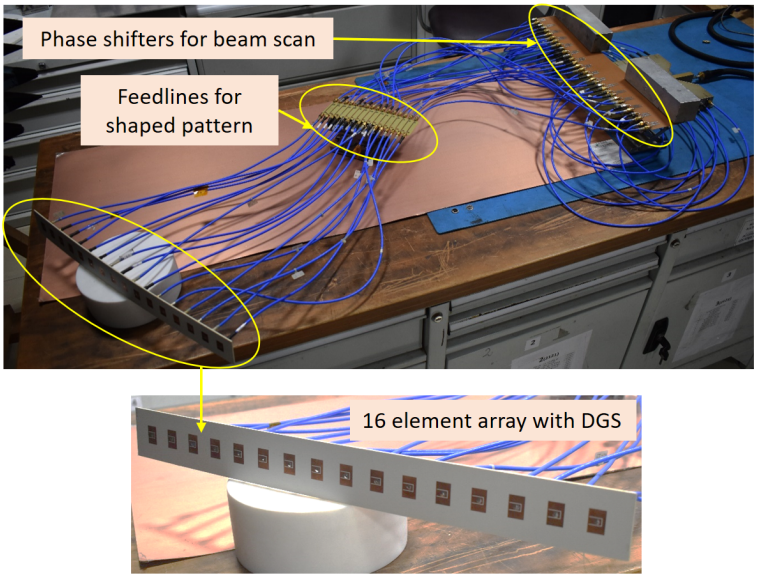

FIGURE 16. Assembly of a 16-element linear array with excitation and phase shifting network.

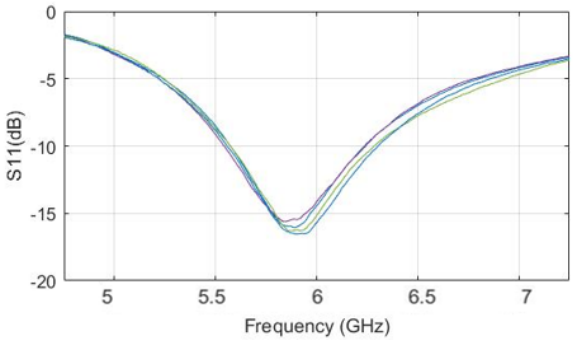

FIGURE 17. Measured return loss of the antenna elements in the developed array.

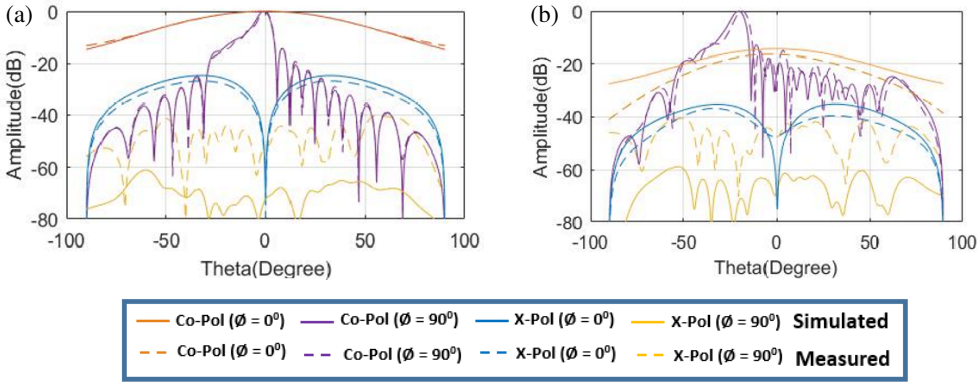

FIGURE 18. Cosecant^2 pattern (a) at 0° and (b) scanned at −20°.

TABLE 5. Efficiency of the proposed antenna.

SN	Antenna Parameters	Value
1	Radiation efficiency (element level)	94.6%
2	Radiation efficiency of the proposed linear array	68%

shows that the element maintained a bandwidth of 330 MHz. The developed array antenna was assembled and integrated with both excitation and phase shifter networks using equiphase cables, as shown in Fig. 16. The radiation pattern of the antenna is measured in an anechoic chamber. The patterns for the 0° and −20° scans are shown in Fig. 18. The simulated radiation pattern was superimposed on the measured patterns for comparison purposes. As shown in Fig. 18, the measured shaped radiation pattern exhibits a 0.3 dB higher ripple than the simulated one, attributed to phase errors introduced by the equiphase cables. Additionally, measured gains of 17.6 dBi for the broadside and 16.3 dBi for the −20° scanned cosecant^2 beam were obtained.

TABLE 6. Comparison table.

Ref.	Frequency	Array Size	Gain (dBi)	Scanning
[10]	5.0 GHz	1 × 18	11.0	No
[12]	28.0 GHz	1 × 12	14.8	No
[13]	6.75 GHz	1 × 32	17.0	No
[P4]	1.0 GHz	1 × 12	12.4	No
This work	6.0 GHz	1 × 16	17.4	Yes

It is important to note that the measured radiation pattern closely matches the simulated pattern. Furthermore, an 8 dB improvement in the array-level cross-polarization was achieved by introducing the DGS. The efficiency of the single element and the proposed 1 × 16 linear array is tabulated in Table 5.

Table 6 compares the developed antenna with those reported in the literature. It shows that the proposed antenna offers better gain performance and scanning capability.

6. CONCLUSION

This paper presents a comprehensive study on the design and implementation of a linear phased-array antenna with a scannable cosecant^2 radiation pattern, specifically aimed at supporting the continuous operation of airborne Synthetic Aperture Radar (SAR) systems while accommodating aircraft motion. U-slots and defective ground structure (DGS) embedded microstrip-based elements are used for the 16-element linear array, offering both bandwidth and cross-polarization improvements. The array achieved a return loss bandwidth of 330 MHz and a gain of 17 dBi in the no-scan condition. Additionally, an 8 dB improvement in the cross-polarization level is reported, which is attributed to the incorporation of the elliptical DGS. To validate the performance of the antenna, a 16-element excitation network and a quadrature hybrid phase shifter were developed. The results underscore the potential of this approach for applications in airborne SAR systems and similar technologies.

REFERENCES

[1] Balanis, C. A., *Antenna Theory: Analysis and Design*, 3rd ed., John Wiley & Sons, 2005.

[2] Bhattacharya, A. K., *Phased Array Antenna*, John Wiley & Sons, 2006.

[3] Mailloux, R. J., *Phased Array Antenna Handbook*, 2nd ed., 2005.

[4] Pozar, D. M., "A relation between the active input impedance and the active element pattern of a phased array," *IEEE Transactions on Antennas and Propagation*, Vol. 51, No. 9, 2486–2489, 2003.

[5] Abdolahi, M., G. Askari, and H. M. Sadeghi, "A new microstrip array antenna with cosecant-squared beam shaping as a radiating column for SSR," in *2014 22nd Iranian Conference on Electrical Engineering (ICEE)*, 1781–1785, Tehran, Iran, 2014.

[6] Mukherjee, A., S. K. Mandal, and R. Ghatak, "Synthesis of non-uniformly spaced planar array geometry using differential evolution algorithm," in *2016 IEEE Indian Antenna Week (IAW 2016)*, 63–66, Madurai, India, 2016.

[7] Dehghani, M. J., Z. Karbalaee, and M. Mahzon, "Design of a wide band antenna array with cosecant square pattern using genetic algorithm," in *2012 20th Telecommunications Forum (TELFOR)*, 564–567, Belgrade, Serbia, 2012.

[8] Yucedag, O. M., M. D. Senturk, and A. S. Turk, "Parametric analysis of open-ended waveguide array feeder for cosecant-squared and pencil beam radiation pattern," in *2012 19th International Conference on Microwaves, Radar & Wireless Communications*, 383–387, Warsaw, Poland, 2012.

[9] Yang, X.-L., L. Chang, J.-Q. Zhang, D. Li, and M. Zhang, "A cosecant squared beam antenna array operating at 5.85-7.6 GHz," in *2019 Cross Strait Quad-Regional Radio Science and Wireless Technology Conference (CSQRWC)*, 1–3, Taiyuan, China, 2019.

[10] Puskely, J., T. Mikulasek, Y. Aslan, A. Roederer, and A. Yarovoy, "5G SIW-based phased antenna array with cosecant-squared shaped pattern," *IEEE Transactions on Antennas and Propagation*, Vol. 70, No. 1, 250–259, Jan. 2022.

[11] Jiang, Y., S. Zhang, Q. Guo, and X. Luan, "A hybrid strategy based on weighting density and genetic algorithm for the synthesis of uniformly weighted concentric ring arrays," *IEEE Antennas and Wireless Propagation Letters*, Vol. 16, 186–189, 2017.

[12] Chu, H., P. Li, and Y.-X. Guo, "A beam-shaping feeding network in series configuration for antenna array with cosecant-square pattern and low sidelobes," *IEEE Antennas and Wireless Propagation Letters*, Vol. 18, No. 4, 742–746, 2019.

[13] Hasibi-Taheri, S., M. Rafaei-Booket, and A. Ghorbani, "Design and fabrication of an efficient metallic phased array for TACAN application," *IEEE Transactions on Antennas and Propagation*, Vol. 68, No. 6, 4979–4984, Jun. 2020.

[14] Cai, X., Q. Zhao, P. Xu, and W. Geyi, "Synthesis of cosecant-squared pattern with a compact linear array using the extended method of maximum power transmission efficiency," *IEEE Antennas and Wireless Propagation Letters*, Vol. 24, No. 4, 863–867, Apr. 2025.

[15] Khandelwal, M. K., B. K. Kanaujia, and S. Kumar, "Defected ground structure: Fundamentals, analysis, and applications in modern wireless trends," *International Journal of Antennas and Propagation*, Vol. 2017, No. 1, 1–22, 2017.

[16] Kumar, G., K. Grover, S. Kulshrestha, S. Chakrabarty, and M. B. Mahajan, "A compact microstrip CP antenna using slots and defected ground structure (DGS)," in *2019 IEEE Indian Conference on Antennas and Propogation (InCAP)*, 1–4, Ahmedabad, India, 2019.

[17] Guha, D., M. Biswas, and Y. M. M. Antar, "Microstrip patch antenna with defected ground structure for cross polarization suppression," *IEEE Antennas and Wireless Propagation Letters*, Vol. 4, 455–458, 2005.

[18] Dwivedy, B., "Consideration of engineered ground planes for planar antennas: Their effects and applications, a review," *IEEE Access*, Vol. 10, 84 317–84 329, 2022.

[19] Shringi, T., V. Sharma, G. Sharma, D. Bhatia, and M. Kumar, "DGS loaded 1×4 patch antenna array for S-band applications," in *2023 Fourth International Conference on Smart Technologies in Computing, Electrical and Electronics (ICSTCEE)*, 1–5, Bengaluru, India, 2023.

[20] Guha, D., C. Kumar, and S. Biswas, *DGS-based Low Cross-pol Array Design and Applications*, 181–203, Wiley, 2023.

[21] Abdullah, M., S. H. Kiani, N. Shoaib, T. Ali, H. Elmannai, A. D. Algarni, and U. F. Khattak, "An eight element wideband DGS MIMO antenna system for 5G handheld devices," *IEEE Access*, Vol. 12, 141 476–141 488, 2024.